Available online at www.sciencedirect.com
ScienceDirect
Ceramics International 38 (2012) 477–485
CERAMICS INTERNATIONAL
www.elsevier.com/locate/ceramint

# Electrochemical corrosion and materials properties of reactively sputtered TiN/TiAlN multilayer coatings

R. Ananthakumar [a], B. Subramanian [a,b,*], Akira Kobayashi [b], M. Jayachandran [a]

[a] CSIR-Central Electrochemical Research Institute, Karaikudi 630 006, India
[b] Joining and Welding Research Institute, Osaka University, Osaka 567 0047, Japan

Received 9 June 2011; received in revised form 14 July 2011; accepted 14 July 2011
Available online 23rd July 2011

**Abstract**

TiN/TiAlN multilayers of 2 μm thickness were successfully prepared by reactive DC magnetron sputtering method. XRD pattern showed the (1 1 1) preferential orientation for both TiN and TiAlN layers. XPS characterization showed the presence of different phases like TiN, $TiO_2$, TiON, AlN and $Al_2O_3$. Cross sectional TEM indicated the columnar growth of the coatings. The average RMS roughness value of 4.8 nm was observed from AFM analysis. TiN/TiAlN coating showed lower friction coefficient and lower wear rate than single layer coatings. The results of electrochemical experiments indicated that a TiN/TiAlN multilayer coating has superior corrosion resistance in 3.5% NaCl solution.


*Keywords:* A. Films; C. Corrosion; E. Cutting tools; E. Wear parts

## 1. Introduction

The multilayer coatings of very low bi-layer thickness received recently special attention because of their increased critical adhesion load. The behavior of such material structures is strongly dependent on the deposition conditions. They are thermodynamically unstable and, therefore, they have to be prepared in a kinetically controlled metastable regime [1]. Polycrystalline multilayers have tremendously high interface-area densities which, in general, lead to increased hardnesses and improved wear resistance. The mechanical properties of the nano-multilayers can be enhanced by the microstructure design, their strengthening mechanism is worthy of further study. In recent years, hard and wear resistant TiN coatings, have gained increasing importance in industry, for example in protecting cutting tools. The application of such coatings is limited to low temperatures since the TiN tends to oxidize at temperatures above about 600 °C, with a rapidly multiplying growth rate of the surface oxide with increasing temperature [2]. As an example, at 700 °C several μm thick oxides form within a few minutes. This can be solved by adding Al atoms to the TiN, forming TiAlN coatings which also have the FCC structure. TiAlN films are attracting more attentions owing to their superior hardness and oxidation resistance compared with the conventional binary transition-metal nitride films, such as TiN, ZrN or CrN, etc. [2].

During high temperature applications of this coating, a very dense and strongly adhesive $Al_2O_3$ film is formed by Al atoms diffusing to the surface, preventing further oxidation [3]. Since TiAlN has a lower thermal conductivity than TiN, more heat is dissipated via chip removal using TiAlN than using TiN. As the thermal loading of the substrate is lower, higher cutting speeds can be obtained by means of TiAlN [4]. In applications at lower temperatures, the performance of TiN is better than that of TiAlN, for example in the case of slow sliding speed or an interrupted cutting process. This is due to differences in brittleness and the friction coefficients of the two materials [5].

PVD coatings can be grown by a number of techniques, including low voltage electric beam evaporation, triode high voltage electric beam evaporation, cathodic arc evaporation, and magnetron sputtering [6]. The magnetron sputtering technique provides the advantages of enhanced adhesion strength of metallic ion etching and the uniform and effective film growth. This technique is now being used in fabrication of commercial coatings as well as laboratory development of new coatings.

In the present work, in an attempt to make a coating with improved mechanical and electrochemical corrosion properties

* Corresponding author. Tel.: +91 4565 227555; fax: +91 4565 227713.
*E-mail address:* subramanianb3@gmail.com (B. Subramanian).

0272-8842/$36.00 
doi:10.1016/j.ceramint.2011.07.030

when compared to those of single-layer TiN and TiAlN coatings, multilayers with individual layers of TiN and TiAlN with the bilayer lengths of 20–30 nm were deposited by reactive magnetron sputtering.

## 2. Experimental methods

TiN/TiAlN multilayered coatings with bilayers lengths of 20–30 nm and thickness of 2 μm were deposited by DC reactive magnetron sputtering using 99.9% pure titanium and titanium aluminum alloy target. Substrates were cleaned in ultrasonic bath using acetone and trichloroethylene. After evacuating the chamber to a base pressure below $10^{-6}$ Torr, the substrate was cleaned by bombarding $Ar^+$ ions with a dc power of 150 W. The TiN and TiAlN were deposited alternatively and the first layer was TiN and the last layer was TiAlN. High purity argon and nitrogen were used as discharge and reactive gases, respectively. A gas manifold was used to distribute $N_2$ gas to each target to a desired $N_2$ partial pressure. By carefully controlling the flow rates of $N_2$ and Ar to each target stoichiometric TiN and TiAlN were obtained simultaneously. Multilayers were formed by depositing TiN in one part of a full rotation of the substrate table and TiAlN in the other part. The bilayer length was varied by changing the rotation speed of the substrate table, with the maximum and minimum time for one rotation being 90 s and 60 s, respectively. The deposition parameters for TiN/TiAlN sputtering are summarized in Table 1.

X-ray diffraction (XRD) studies were performed with a PANalytical X'Pert Pro powder diffractometer using CuKα radiation. Chemical composition was determined by X-ray photoelectron spectroscopy (XPS) and energy dispersive X-ray analysis (EDX) methods. The XPS measurements were taken at a base pressure of $10^{-8}$ Torr using MgKα (X-ray of 1253.6 eV source) type Multilab 2000. The elemental composition of the films was obtained by EDX analysis using a FESEM. The surface morphology of the films was studied using field emission scanning electron microscope (FESEM, sirion FEI). Nanoscale studies of the structure and the surface roughness of the deposited films were also investigated by atomic force microscopy (AFM). The Raman spectroscopy measurements were used as excitation wavelength of 632.8 nm. The data were collected with a 10 s data point acquisition time in the spectral region of 200–1000 $cm^{-1}$.

A block on ring testing machine was employed to assess the wear resistance of the multilayer coatings. The experimental conditions were an applied load of 400 g or 3.924 N, a sliding speed of 100 rpm and the ring material, having a diameter of 60 mm, which was made of high chromium high carbon tool steel with Vickers hardness 850 HV. The wear rate was calculated by measuring the weight change of a specimen before and after the test.

The corrosion behavior was determined by electrochemical potential–current density measurements. A potentiostat (Autolab PGSTAT galvanostat/potentiostat) was employed to realize the corrosion experiments. A conventional three-electrode cell was used with the counter electrode made of a platinum rod and a saturated calomel electrode (SCE) as a reference electrode and the sample as the working electrode. The test electrolytes for electrochemical investigations were 3.5% NaCl solutions held at room temperature. The test specimens were masked with 3 M scotch to expose a constant surface area of 1 $cm^2$. Different electrochemical techniques were used to characterize the behavior of the TiN/TiAlN multilayered coatings and coated steel samples. In order to establish the open circuit potential (OCP), prior to the polarization measurements, the samples were immersed in the solution for about 60 min. The applied alternating potential had root mean square amplitude of 10 mV on the OCP. After getting the stable OCP, the upper and lower potential limits of linear sweep voltammetry were set at +200 and −200 mV respectively with reference to OCP. The sweep rate was 1 mV $s^{-1}$. The corrosion potential $E_{corr}$, corrosion current $I_{corr}$ and corrosion rate was determined by the Tafel extrapolation method. Impedance measurements were conducted using a frequency response analyzer and the

Table 1
Deposition parameters for TiN/TiAlN reactive sputtering.

| Objects | Specification |
|---|---|
| Target (2''Dia) | Ti (99.9%) and TiAl (99.9%) |
| Substrate | MS, Glass |
| Target to substrate distance | 60 mm |
| Ultimate vacuum | $1 \times 10^{-6}$ mbar |
| Operating vacuum | $2 \times 10^{-3}$ mbar |
| Sputtering gas ($Ar:N_2$) | 2:1 |
| Power | 150 W |
| Substrate temperature | 400 °C |

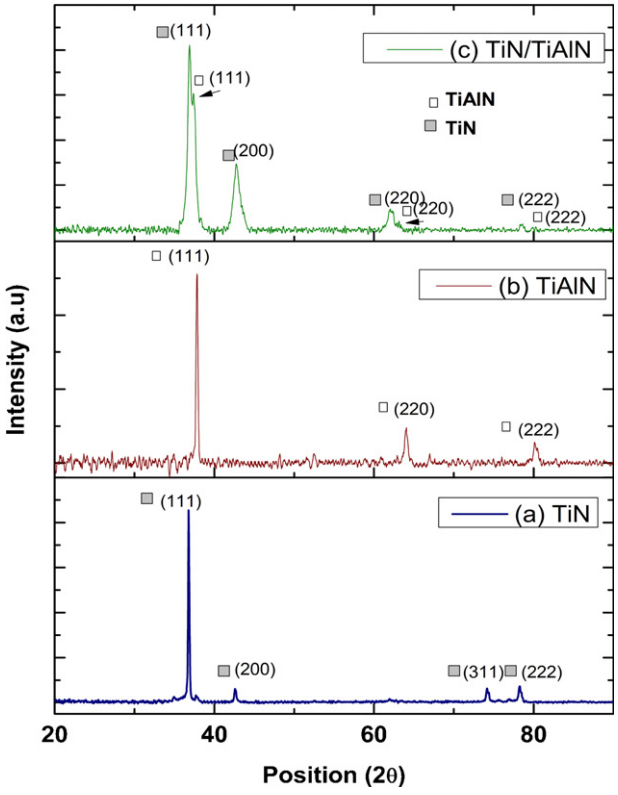


Fig. 1. XRD patterns of TiN/TiAlN multilayers prepared by magnetron sputtering.

spectrum was recorded in the frequency range 10 MHz to 100 kHz.

## 3. Results and discussion

### 3.1. Structure, microstructure and compositional analysis

Typical X-ray diffraction pattern of single layer TiN (Fig. 1a), TiAlN (Fig. 1b) and TiN/TiAlN (Fig. 1c) multilayered coatings deposited on steel substrate at substrate temperature of 400 °C is shown in Fig. 1. TiN and TiAlN single layers are polycrystalline exhibiting diffraction peaks with the preferred orientation along (1 1 1) plane. Both TiN and TiAlN showed a single-phase fcc structure [7]. It is noted that the cubic TiAlN B1 NaCl structure has the same Bravais lattice (crystal structure) of the cubic TiN structure. The peak positions of TiAlN coatings are shifted to the higher angles with respect to TiN peaks owing to lattice constant decreases arise from the

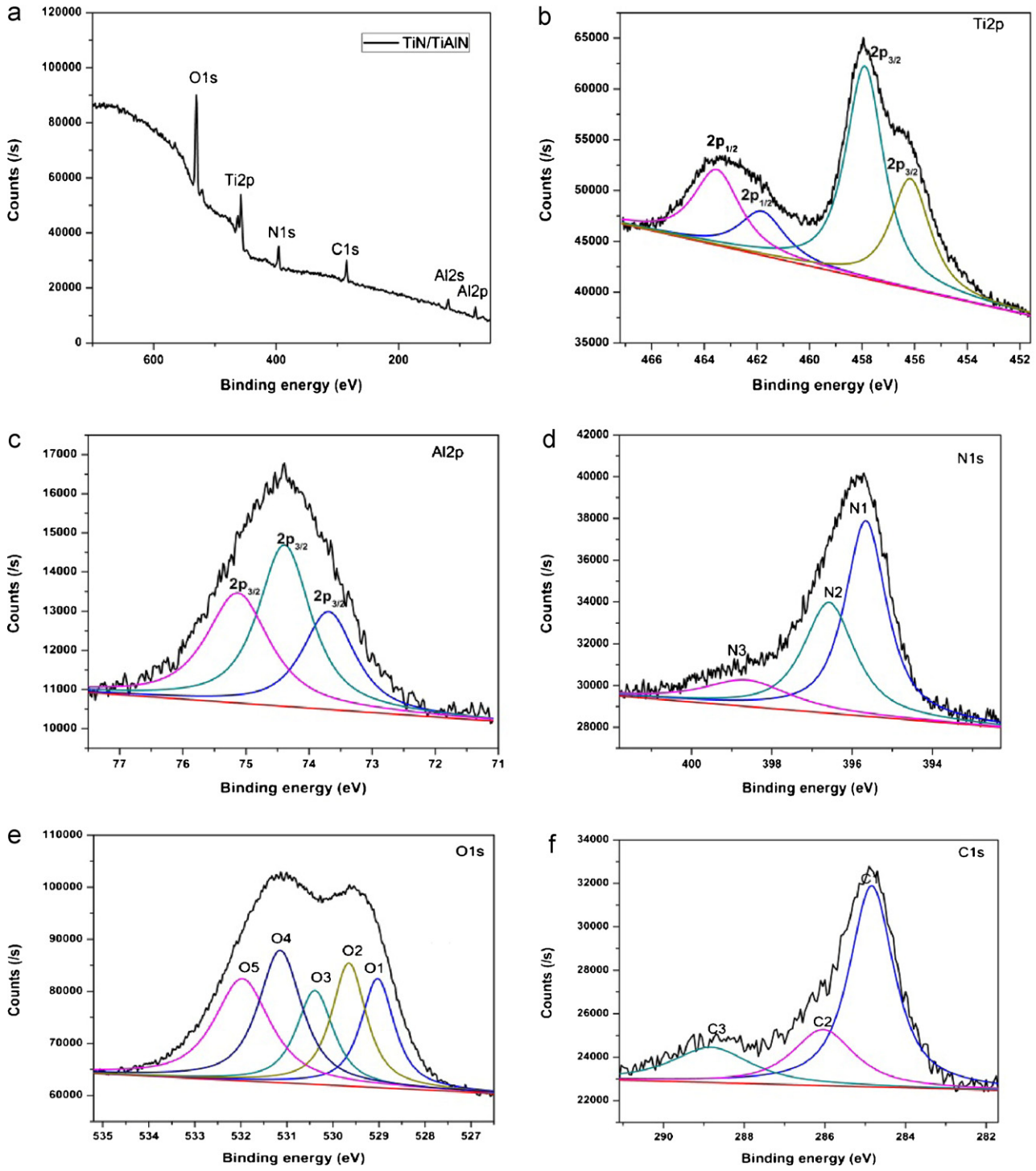


Fig. 2. XPS spectra of TiN/TiAlN multilayer coatings deposited at 400 °C (a) survey (b) Ti 2p (c) Al 2p (d) N 1s (e) O 1s (f) C 1s.

partial replacement of the titanium atoms in the TiN lattice by the aluminum. The TiN/TiAlN multilayer coating also exhibited the B1–NaCl crystal structure. Diffraction peaks of (1 1 1), (2 0 0), (2 2 0) and (2 2 2) for TiN and (1 1 1) (2 2 0) and (2 2 2) for TiAlN peaks [8] respectively, were observed in the XRD pattern.

Fig. 2 shows the XPS spectra of TiN/TiAlN films. The deposited films were cleaned before XPS analysis to prevent them from contamination by adventitious oxygen. The analysis of XPS survey spectra indicates (Fig. 2a) that Ti, Al, N, O and C elements coexist in the deposited TiN/TiAlN films. The peak associated with Ti 2p consists of two peaks centered at 457.7 (Ti 2p3/2) and 462.7 eV (2p1/2). Gauss fitting of Ti 2p3/2 peak indicated (Fig. 2b) that it consisted of two peak centered at 456.1 and 457.9 eV which can be attributed to chemical bonds of TiON and $TiO_2$ respectively [9]. Moreover, the 2p1/2 envelopes are in 461.1 eV for TiN and 463.5 eV for $TiO_2$ compound [9].

Fig. 2c shows the XPS spectra for the corresponding Al 2p3/2 core levels of sample. The major contribution in Fig. 2c centered at 73.6 eV, is assigned to Al 2p3/2 in $Al_2O_3$ bonds [10]. The major binding energy contribution at 74.3 eV is accredited to Al–N chemical bonding which in very good accordance with most reports [11], while the lower binding energy contribution at 75.1 eV is assigned to Al–O bonding, of reported binding energies [10].

The N 1s spectrum of the TiN/TiAlN multilayered coatings in Fig. 2d presents an asymmetric shape. An obvious shoulder can be seen at higher binding energy side of the main peak. Three peaks can be found after the Gaussian multipeak fitting for the N 1s spectrum. The main peak position of 396.5 eV corresponds to the N 1s electron in TiN [12]. The other contribution of the N 1s core level, in Fig. 2d of the sample, centered at 398.6 eV, is assigned to N–Al bonding. The peak at 395.6 eV assigned to N–C bonding which is in the form of $TiO_xN_y$ [13].

The O 1s XPS peak of TiN/TiAlN multilayer coatings to be fitted by the five Gaussian curves centered at 529.0, 529.6, 530.3, 531.1 and 531.9 eV (Fig. 2e). The components centered at 529.0, 529.6 and 531.1 eV are assigned to $TiO_2$, Ti–O and Ti–O bulk, OH respectively [12]. A peak, located at 530.3 eV correspondents to Al–O [14] bonding in $Al_2O_3$ species. Another component of the O 1s transition of minor intensity, at 531.9 eV, may be associated to physically adsorbed [12] molecular $H_2O$. The C 1s spectrum of as deposited films (Fig. 2f) shows peaks at 284.8, 286.0 and 288.8 eV, which are assigned to C (or CH), C–N and C=O, respectively [15].

The elemental composition of the TiN/TiAlN multilayer coatings was determined by EDX technique. An EDX spectrum of a TiN/TiAlN film shows (Fig. 3) the presence of the Ti, Al, N, and Si elements in the ratio of 62.12%, 18.17%, 9.37% and 10.33% respectively.

Raman spectra of as deposited TiN, TiAlN single layer and TiN/TiAlN multilayer coatings are shown in Fig. 4. TiN coatings exhibited the characteristic peaks at 209 and 318 $cm^{-1}$ for longitudinal acoustic (LA) and transverse acoustic (TA) modes and 567 $cm^{-1}$ for transverse optic (TO) and longitudinal optic (LO) mode. Scattering in the acoustic range is primarily determined by the vibrations of the Ti ions and that in the optic range by the vibrations of the N ions. The spectrum in the acoustic frequency range (200–300 $cm^{-1}$) is mainly due to the vibrations of metal atoms, whereas the vibrations of lighter non-metal ions dominate the optical range (400–650 $cm^{-1}$) [16]. The Raman spectrum of TiAlN coating consists of two broadbands centered at 253 and 673 $cm^{-1}$ which is similar to that of TiN in which some of the Ti atoms of larger radii are replaced by smaller Al atoms. The TiN/TiAlN multilayer coatings displayed one strong and one weak broad bands center at about 244 and 626 $cm^{-1}$ which can be associated to acoustic and optic modes of vibration [17] due to Ti and N.

The microstructure and morphology of the films have been observed by scanning electron microscopy (SEM), transmission electron microscope (TEM) and atomic force spectroscopy (AFM). Fig. 5a presents the morphology of the coatings prepared at 400 °C. It can be seen that the film exhibits a cell-like surface appearance with an average grain size of about

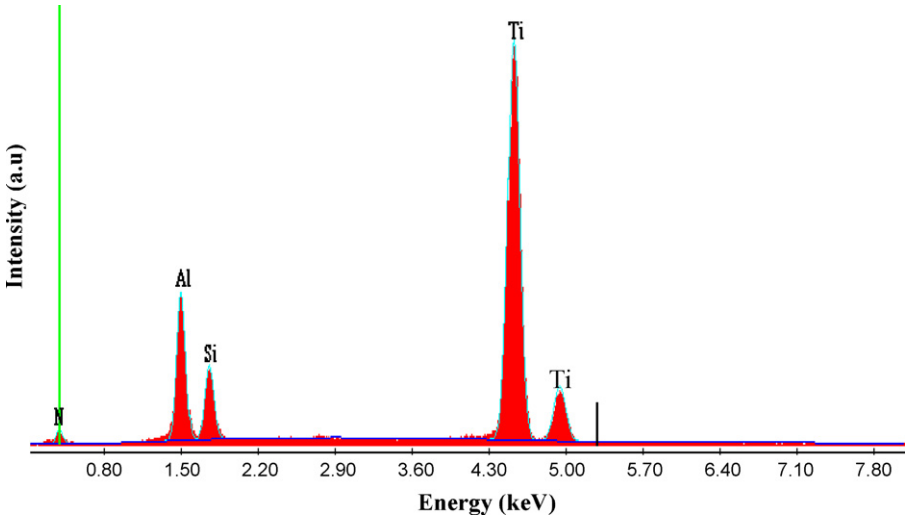


Fig. 3. EDX spectrum of TiN/TiAlN multilayer coating.

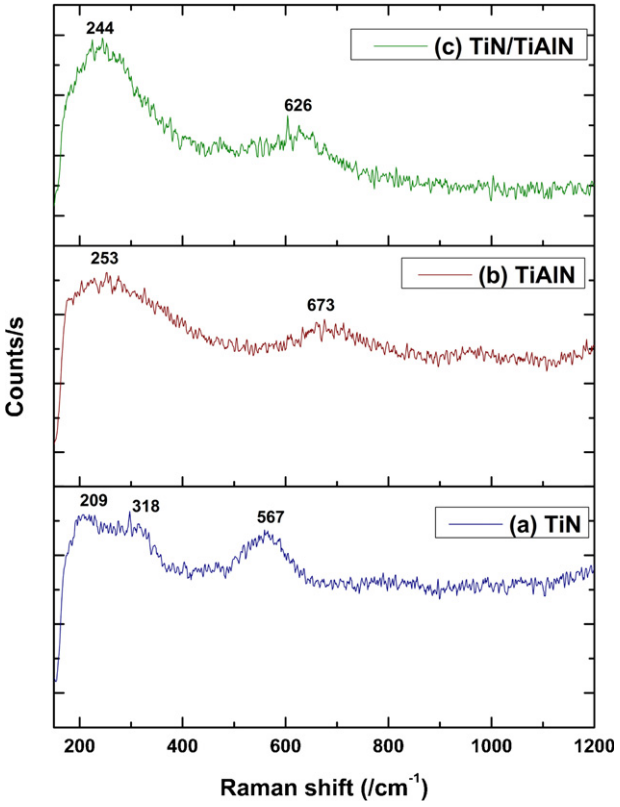


Fig. 4. The Raman spectra of TiN/TiAlN multilayer coatings.

60 nm. A close look at the micrograph indicates that the cells are composed of tiny grains. High resolution cross sectional TEM analysis (Fig. 5b) showed the columnar growth of the coating. The polycrystalline diffraction pattern (Fig. 5c) confirms the information provided by X-ray diffraction.

From Fig. 5d the growth model of TiN/TiAlN multilayered coatings appears as the island growth. The growth orientation of grain shows uprightness to the substrate surface. The surface of TiN/TiAlN coatings is very smooth. The average RMS roughness value of 4.8 nm was observed.

### 3.2. Wear and electrochemical corrosion properties

The frictional behavior of the coatings under a normal load of 3.924 N at room temperature is shown in Fig. 6a. Sliding friction for TiN/TiAlN coated films shows a relatively lower value of about 0.25 compared to the 0.40 and 0.45 for the single layer coatings and bare substrate. TiN/TiAlN multilayered coatings show the lowest coefficient of friction compared to single layer and bare substrate. In Fig. 6b a large difference can be seen in wear rate and found to be the lowest for the TiN/TiAlN multilayer coatings.

A lower coefficient of friction reported for the TiN/TiAlN multilayer system (Fig. 6a) can be correlated to the exposure of the TiAlN layer to the atmosphere, leading to improved tribological properties of the multilayer coating [18]. The enhanced wear resistance of TiN/TiAlN multilayer coatings can be attributed to many factors such as high hardness, formation of $Al_2O_3$ (commonly known as tribo-oxidation) on the worn surface, and decreases in the coefficient of friction. The

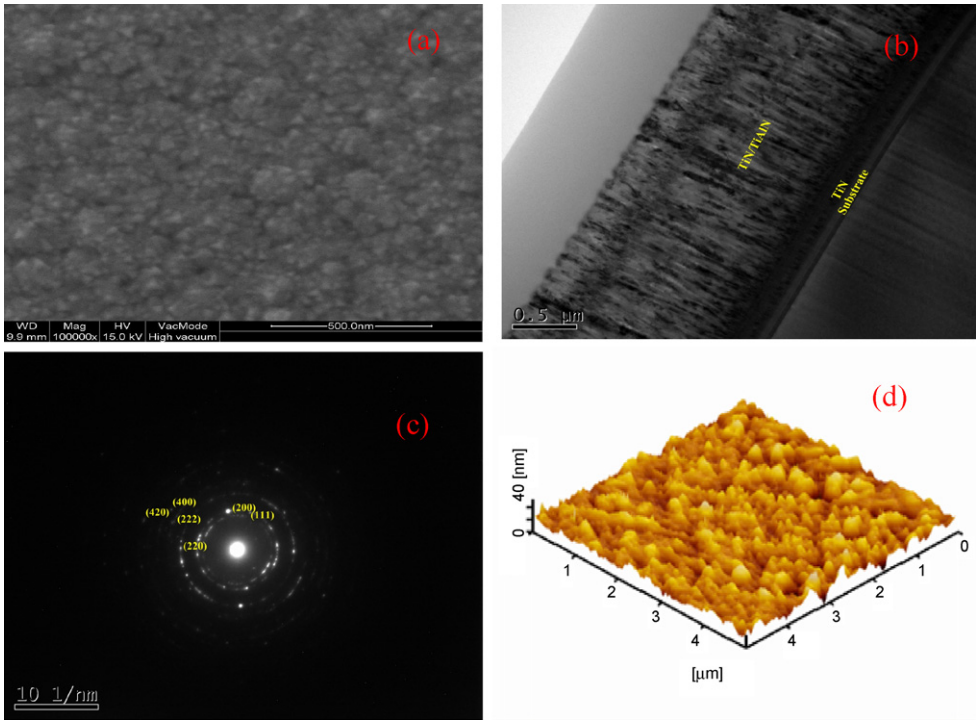


Fig. 5. (a) FESEM image of TiN/TiAlN coatings (b) Cross sectional TEM image of TiN/TiAlN coatings (c) Typical 3D AFM image of TiN/TiAlN multilayered coatings (d) SAED pattern of TiN/TiAlN coatings.

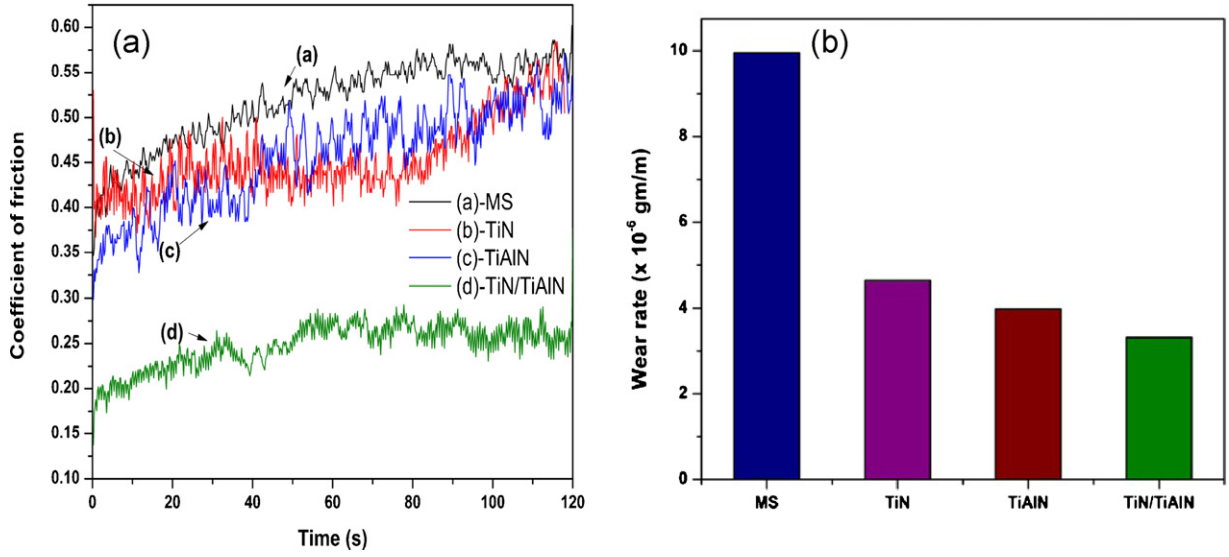


Fig. 6. (a) Friction coefficient of the TiN/TiAlN multilayer coatings. (b) Wear rate for TiN/TiAlN multilayer coatings.

aluminum oxide layer helps to build an additional protective coating on the worn surface, thus, improving the wear resistance. A decrease in the wear volume with an increase in the hardness has been reported and has been explained in terms of the Archard relationship in which the wear volume is inversely proportional to the hardness of the worn surface [19,20]. The interfaces in a multilayer coating act as crack inhibitors, thereby increasing the fracture resistance due to crack deflection at the interfaces, crack tip shielding by plastic deformation, residual stress distribution, etc. [21]. The multilayer system not only increases the load carrying capacity but also improves the fatigue strength of the coating/substrate system.

Potentiodynamic polarization curves of the TiN/TiAlN multilayer, TiAlN, TiN single layer coatings and the bare substrate are shown in Fig. 7. The corrosion current density and the corrosion potential were obtained by the intersection of the extrapolation of anodic and cathodic Tafel curves. The corrosion potential of the steel substrate is about −0.837 V. The $E_{corr}$ of multilayer layer coated samples, when compared to the single layers and substrate, shows a shift towards the positive side. The positive shift of $E_{corr}$ (−0.837 to −0.546 V for TiN/TiAlN) indicates better corrosion resistance of the TiN/TiAlN multilayer coatings. The corrosion current density of the multilayer and single layer coatings was found much lower than that of the bare substrate. The TiN/TiAlN multilayered coating has performed very well and showed superior corrosion resistance on the basis of corrosion current density and the corrosion potential. The corrosion resistance of TiAlN is better than TiN because addition of third element (such as Al) to the transition metal nitrides improves the corrosion resistance [22]. During the chemical attack Al easily forms $Al_2O_3$ layer on the surface of the coating, which passivates the surface and prevents further corrosion attack [23]. The presence of a passive layer leads to an additional resistance to the corrosive medium passing through the pores. In addition, TiN exhibits the columnar structure with pores between the inter-granular columns, forming a direct path for the corrosive medium to pass through the coating defects [24]. As the number of interface increases, more numbers of micro-pores are blocked. This improves the corrosion resistance of the multilayer coatings, when compared to single layer coatings.

From the polarization test results, the protective efficiency, $P_i$ (%) of the films can be calculated by Eq. (1)

$$P_i(\%) = \left[1 - \left(\frac{i_{corr}}{i^0_{corr}}\right)\right] \times 100 \quad (1)$$

where $i_{corr}$ and $i^0_{corr}$ indicate the corrosion current density of the film and substrate, respectively [25]. The TiN/TiAlN multilayered coating shows the highest protective efficiency of 96.47%

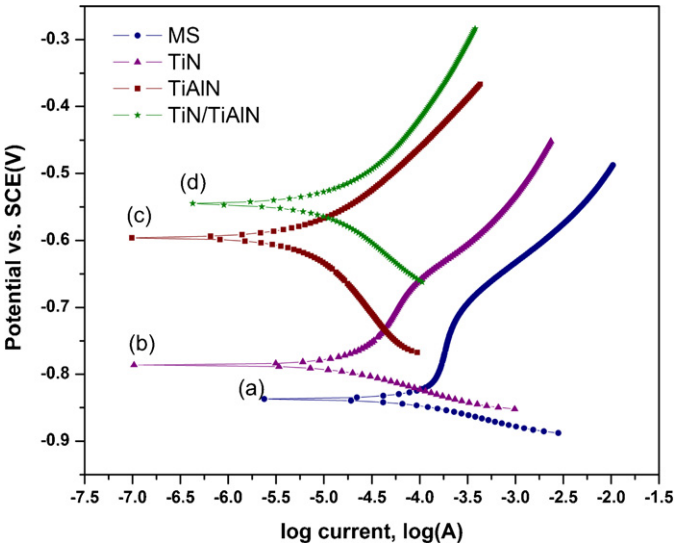


Fig. 7. Polarization studies of (a) Mild steel substrate (b) TiN film (c) TiAlN film and (d) TiN/TiAlN multilayered film in 3.5% NaCl solution.

caused by lowest corrosion current density of $0.041 \times 10^{-5}$ μA/cm$^2$, compared to single layer TiN and TiAlN coatings.

In PVD deposition the coating defects, such as pinholes and porosity usually occur. These defects could weaken the interfacial material and provide easy fracture path for adhesion failure between substrate and the corrosive medium. This porosity was calculated from $E_{corr}$ and $R_p$ measurement deduced from the potentiodynamic polarization technique using the relation [26].

$$P = \left(\frac{R_{ps}}{R_p}\right) \times 10^{-\Delta E_{corr}/b_a} \quad (2)$$

where $P$ is the total coating porosity, $R_{ps}$ is the polarization resistance of the uncoated substrates, $R_p$ is the polarization resistance of the coated substrate, $\Delta E_{corr}$ the difference between the corrosion potentials of the coated and uncoated substrate, and $b_a$ is the anodic Tafel slope of the substrate. Porosity of the TiN/TiAlN ($2.232 \times 10^{-2}$%) multilayer coatings showed lower value compare to TiAlN ($1.998 \times 10^{-1}$%) and for the TiN (7.27%) single layers coatings.

Fig. 8 shows the Nyquist plots for TiN/TiAlN multilayer, TiN, TiAlN, single layer coatings and steel substrate. The Nyquist plots shows $R_{ct}$ value increases and $C_{dl}$ value decreases in the following order: uncoated substrate, TiN, TiAlN and TiN/TiAlN multilayer coated samples.

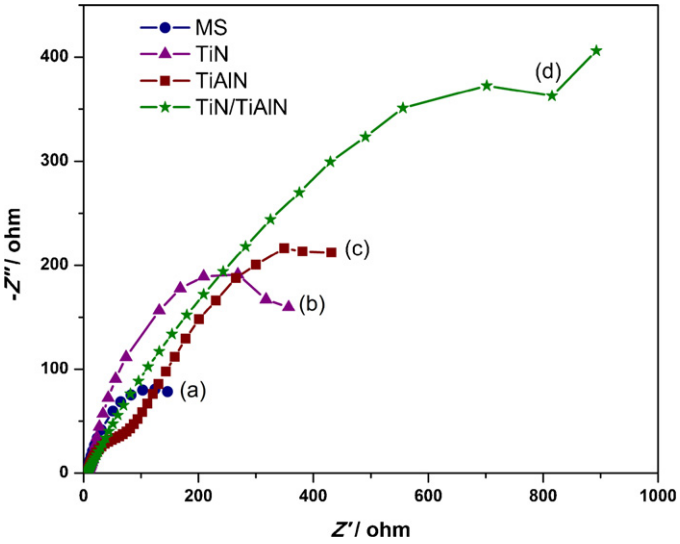


Fig. 8. Nyquist plot of (a) Mild steel substrate (b) TiN film (c) TiAlN film and (d) TiN/TiAlN multilayered film in 3.5% NaCl solution.

SEM micrographs of the substrate, TiN, TiAlN single layer, and TiN/TiAlN multilayer coatings after corrosion test are shown in Fig. 9. More number of defects and corrosion products are observed in the bare 316L stainless steel substrate and they are shown in Fig. 9a. Fine pits are distributed throughout the

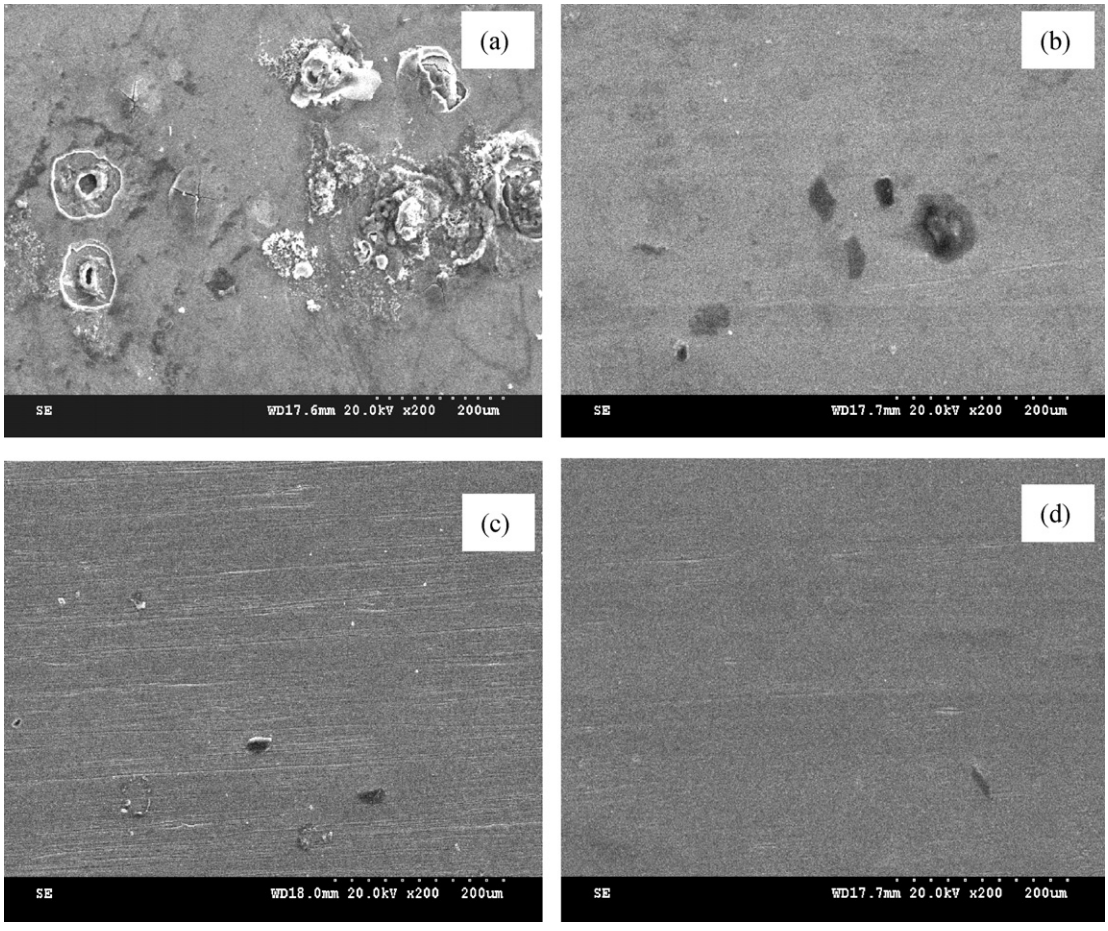


Fig. 9. SEM surface morphology of (a) MS, (b) TiN, (c) TiAlN single layer and (b) TiN/TiAlN multilayered coatings after corrosion testing in 3.5% NaCl solution.

surface as a result of the localized corrosion attack. For TiN coating (Fig. 9b), it is clearly shown that the surface exhibits several pinhole morphology. This could be because of the columnar microstructure of the sputtered TiN coatings containing a lot of micropores which leads to accelerated corrosion. The corrosion pit is fully open, which could be due to the flaking of the coating as a result of the chemical attack. The corrosion underneath the coating causes rust formation and consequently increases the interface volume, which results in delamination of the coating. In the case of TiAlN (Fig. 9c) single layer coatings, only fewer corrosion products could be observed because of the formation of the stable but thin $Al_2O_3$ on the surface of the coating. Fig. 9d shows the surface morphology of TiN/TiAlN multilayer coatings. In corroboration with the results of electrochemical characterization, a good corrosion resistance of this coating is evident from the absence of corrosion products. This is due to the fact that most of the micro-pores are blocked as a result of successive deposition of the materials.

## 4. Conclusions

In conclusion the TiN/TiAlN multilayered coatings were fabricated using reactive DC magnetron sputtering in the Ar and $N_2$ gas mixture. XRD examinations revealed that TiN/TiAlN multilayer coatings had a cubic structure with (1 1 1) preferential orientation. From XPS spectra, Ti 2p3/2 peak consisted of two peak centers at 456.1 and 457.9 eV which can be attributed to chemical bonds of TiON and $TiO_2$ respectively. Raman spectra exhibited the characteristic peaks at 244 and 626 $cm^{-1}$. Morphology of the film exhibits a cell-like surface appearance with an average grain size of about 60 nm was observed. In addition, TiN/TiAlN multilayer coatings show the lowest average friction coefficient against steel compared to single layer coated substrate and bare substrate. The TiN/TiAlN multilayered coating shows the highest protective efficiency of 96.4%. The protective ability of the film was found to be superior for TiN/TiAlN multilayer coatings compared to the single layers TiN and TiAlN coatings. The results of this study indicated that TiN/TiAlN multilayers can improve the corrosion and wear behavior of bare steel substrates.

## Acknowledgement

One of the authors (B.S.) thanks the Japan Society for the Promotion of Science, Japan for the award of FY 2011 JSPS Long term Invitation Fellowship and the Department of Science & Technology, New Delhi, for a research grant under SERC Scheme No. SR/S1/PC/31/2008.

## References

[1] R. Manaila, A. Devenyi, D. Biro, L. David, P.B. Barna, A. Kovacs, Multilayer TiAlN coatings with composition gradient, Surface and Coating Technology 151–152 (2002) 21–25.
[2] J. Yue, G. Li, Microstructure and mechanical properties of TiAlN/$Si_3N_4$ nano-multilayers synthesized by reactive magnetron sputtering, Journal Alloys and Compounds 481 (1–2) (2009) 710–713.
[3] V.K. William Grips, H.C. Barshilia, V. Ezhil Selvi, Kalavati, K.S. Rajam, Electrochemical behavior of single layer CrN, TiN, TiAlN coatings and nanolayered TiAlN/CrN multilayer coatings prepared by reactive direct current magnetron sputtering, Thin Solid Films 514 (1–2) (2006) 204–211.
[4] S.J. Suresha, R. Bhide, V. Jayaram, S.K. Biswas, Processing, microstructure and hardness of TiN/(Ti, Al)N multilayer coatings, Materials Science and Engineering A 429 (1–2) (2006) 252–260.
[5] K.N. Andersen, E.J. Bienk, K.O. Schweitz, H. Reitz, J. Chevallier, P. Kringhøj, J. Bøttiger, Deposition microstructure and mechanical and tribological properties of magnetron sputtered TiN/TiAlN multilayers, Surface and Coating Technology 123 (2–3) (2000) 219–226.
[6] Q. Luo, W.M. Rainforth, W.D. Münz, TEM observations of wear mechanisms of TiAlCrN and TiAlN/CrN coatings grown by combined steered-arc/unbalanced magnetron deposition, Wear 225–229 (1999) 74–82.
[7] Li Chen, Yong Du, Fei Yin, Jia Li, Mechanical properties of (Ti, Al)N monolayer and TiN/(Ti, Al)N multilayer coatings, International Journal of Refractory Metals & Hard Materials 25 (2007) 72–76.
[8] G. Bejarano Gaitan, J.C. Caicedo, Adam G. Balogh, S. Gottschalk, Cutting tools performance enhancement by using a TiN/TiAlN multilayer coating system, Physica Status Solidi C 11 (2007) 4260–4266.
[9] B. Subramanian, R. Ananthakumar, V.S. Vidhya, M. Jayachandran, Influence of substrate temperature on the materials properties of reactive DC magnetron sputtered Ti/TiN multilayered thin films, Materials Science and Engineering B 176 (1) (2011) 1–7.
[10] L. Rosenberger, R. Baird, F. McCullen, G. Auner, G. Shreve, XPS analysis of aluminum nitride films deposited by plasma source molecular beam epitaxy, Surface and Interface Analysis 40 (2008) 1254–1261.
[11] B. Subramanian, R. Ananthakumar, M. Jayachandran, Microstructural, mechanical and electrochemical corrosion properties of sputtered titanium–aluminum–nitride films for bio-implants, Vacuum 85 (5) (2010) 601–609.
[12] J.F. Marco, J.R. Gancedo, M.A. Auger, O. Sanchez, J.M. Albella, Chemical stability of TiN, TiAlN and AlN layers in aggressive $SO_2$ environments, Surface and Interface Analysis 37 (2005) 1082–1091.
[13] A.C. Agudelo, J.R. Gancedo, J.F. Marco, D. Hanzel, Corrosion resistance of titanium nitride and mixed titanium/titanium nitride coatings on iron in humid $SO_2$-containing atmospheres, Journal of Vaccum Science and Technology A 15 (1997) 3163–3169.
[14] C.D. Wagner, D.E. Passoja, H.F. Hillery, T.G. Kinisky, H.A. Six, W.T. Jansen, J.A. Taylor, Auger and photoelectron line energy relationships in aluminum–oxygen and silicon–oxygen compounds, Journal of Vacuum Science and Technology 21 (1982) 933–944.
[15] M. Balaceanu, M. Braic, D. Macovei, M.J. Genet, A. Manea, D. Pantelica, V. Braic, F. Negoita, Properties of titanium based hard coatings deposited by the cathodic arc method, I. Microchemical and microstructural characteristics, Journal of Optoelectronics and Advanced Materials 4 (2002) 107–114.
[16] C.P. Constable, J. Yarwood, W.D. Munz, Raman microscopic studies of PVD hard coatings, Surface and Coating Technology 116–119 (1999) 155–159.
[17] P.W. Shum, K.Y. Li, Z.F. Zhou, Y.G. Shen, Structural and mechanical properties of titanium–aluminium–nitride films deposited by reactive close-field unbalanced magnetron sputtering, Surface and Coating Technology 185 (2–3) (2004) 245–253.
[18] M. Nordin, M. Larsson, S. Hogmark, Mechanical and tribological properties of multilayered PVD TiN/CrN, Wear 232 (1999) 221–225.
[19] J. An, Q.Y. Zhang, Structure, hardness and tribological properties of nanolayered TiN/TaN multilayer coatings, Materials Characterization 58 (2007) 439–446.
[20] J.F Archard, Contact and rubbing of flat surfaces, Journal of Applied Physics 24 (1953) 981–988.
[21] Y.M. Zhou, R. Asaki, K. Higashi, W.H. Soe, R. Yamamoto, Sliding wear behavior of polycrystalline TiN/CrN multilayers against an alumina ball, Surface and Coating Technology 130 (2000) 9–14.
[22] H. Alanyani, R.M. Souto, Research on the corrosion behavior of TiN–TiAlN multilayer coatings deposited by cathodic-arc ion plating, Corrosion 59 (2003) 851–854.

[23] L. Cunha, M. Andritschky, L. Rebouta, K. Pischow, Corrosion of CrN and TiAlN coatings in chloride-containing atmospheres, Surface and Coating Technology 116 (1999) 1152–1160.
[24] R. Brown, M.N. Alias, R. Fontana, Effect of composition and thickness on corrosion behavior of TiN and ZrN thin films, Surface and Coating Technology 62 (1993) 467–473.
[25] Y.H. Yoo, D.P. Le, J.G. Kim, S.K. Kim, P.V. Vinh, Corrosion behavior of TiN, TiAlN, TiAlSiN thin films deposited on tool steel in the 3.5 wt.% NaCl solution, Thin Solid Films 516 (2008) 3544–3548.
[26] B. Elsener, A. Rota, H. Bohni, Impedance study on the corrosion of PVD and CVD titanium nitride coatings, Mater. Sci. Forum 44/45 (1989) 29–38.